Mechatronics and Intelligent Transportation Systems
https://www.acadlore.com/journals/MITS

Management Analysis and Control Strategies for the Road Incident Dynamics Model

Mehboob Ali[1], Wasi Ur Rahman[2*], Zubir Shah[3]

[1] School of Mathematics and Physics, Guangxi Minzu University, 530006 Nanning, China
[2] Department of Mathematics, Shaheed Benazir Bhutto University Sheringal, 18000 Dir Upper, Pakistan
[3] Department of Statistics, Abdul Wali Khan University, 23200 Mardan, Pakistan

* Correspondence: Wasi Ur Rahman (wasi@sbbu.edu.pk)

Received: 12-28-2025 **Revised:** 03-02-2026 **Accepted:** 03-15-2026

Citation: M. Ali, W. Ur Rahman, and Z. Shah, "Management analysis and control strategies for the road incident dynamics model," *Mechatron. Intell Transp. Syst.*, vol. 5, no. 1, pp. 71–85, 2026. https://doi.org/10.56578/mits050105.

Abstract: This paper presented a two-vehicle rear-end collision dynamics model for analyzing crash mechanisms in urban traffic and proposed response and control strategies to mitigate secondary congestion and improve post-incident traffic recovery. Rear-end collisions are among the most frequent crash types in urban road networks. They disrupt traffic flow and increase travel delays, fuel consumption as well as emissions, hence triggering secondary crashes if not handled properly. Accurate dynamic modeling of two-vehicle rear-end collisions is essential for improving traffic safety, efficiency of responding to incidents, and design of the vehicle control system. The model mathematically represented the interaction between a leading vehicle and a following vehicle during pre-impact, impact, and post-impact phases. It incorporated conservation of momentum, restitution characteristics, braking dynamics, and vehicle mass properties. The study further examined how response strategies such as rapid clearance, lane management, and adaptive traffic control affected congestion dissipation and traffic recovery. The analysis demonstrated that accurate dynamics modeling enabled reliable estimation of impact severity, post-collision velocities, and clearance time. Optimized response management significantly reduced secondary congestion, shortened traffic recovery time, and enhanced overall roadway performance. The study integrated mechanical collision dynamics with traffic management interventions within a unified analytical framework. Unlike purely traffic-flow-based models, this approach directly linked physical crash mechanics with network-level congestion propagation and response optimization. Future research will extend the model to multi-vehicle chain collisions, incorporate stochastic drivers' reaction time and braking behavior, and integrate the framework with intelligent transportation systems under dynamic urban traffic conditions.

Keywords: ABCDS deterministic model; Threshold number; Stability analysis; Sensitivity analysis; Optimal control

1 Introduction

The rapid growth of urban traffic has led to improved vehicle density, congestion, and a higher frequency of traffic accidents. Among various crash types, rear-end collisions represent one of the most common incidents in urban road networks. These collisions not only pose significant safety risks but also contribute to traffic disruptions, increased fuel consumption, environmental pollution, and secondary crashes. This study explores an AI-driven approach to enhance sustainability in urban public transportation by optimizing efficiency, reducing emissions, and promoting smarter mobility solutions [1, 2]. Mathematical modeling plays a crucial role in studying the mechanisms of rear-end collisions. A two-vehicle rear-end collision typically involves the dynamic interaction between a leading vehicle and a following vehicle during pre-impact, impact, and post-impact phases. Recent research has explored modeling vehicular movements at intersections using optimal control techniques to improve traffic efficiency and safety [3, 4]. These analytical approaches allow researchers to estimate impact severity, post-collision velocities, stopping distances, and crash results under varying traffic conditions [5]. Rear-end collision models should account for the dynamic nature of traffic flow, where vehicle speeds, headways, drivers' reaction time, and road conditions vary continuously [6]. Advanced models integrate traffic flow theory, car-following performance, and braking response mechanisms to represent the interaction between vehicles more realistically [7, 8]. Optimization of vehicle

routing, particularly with time windows, has been extensively studied to improve operational efficiency and reduce environmental impact, providing key insights for AI-driven enhancements in urban public transportation. Heuristic optimization methods, such as tabu search, have been successfully applied to dynamic transportation problems, including patient transfers between care units, demonstrating the potential of AI-based strategies to improve routing efficiency and resource utilization in complex urban transportation systems [9, 10]. A critical aspect of rear-end collision modeling is the prediction of the occurrence and severity of collisions. The effectiveness of such models is contingent on accurately capturing relative velocity, inter-vehicle arrangement, and deceleration behavior. Recent advances in demand-responsive transport leverage mobile data analytics to optimize urban mobility, offering AI-driven solutions that enhance the efficiency, adaptability, and sustainability of public transportation systems [10].

With the increasing availability of real-time traffic data from sensors, Global Positioning System (GPS) devices, and associated vehicle technologies, data-driven and machine learning approaches are being combined with classical dynamic models to enhance predictive accuracy. AI-driven approaches are transforming urban public transportation by improving efficiency, sustainability, and adaptability. Studies on intersection control. AI-driven methods, including neural network-based optimization for feeder bus routes, have shown promise in improving efficiency and sustainability in urban public transportation [11]. Collision dynamics modeling also supports the development of active security systems, such as adaptive cruise control (ACC) and autonomous emergency braking (AEB). Optimization algorithms are employed to design control strategies that minimize collision risks while maintaining the stability of traffic flow. Machine learning techniques have also been applied to short-term demand prediction in bike-sharing services, supporting more efficient and sustainable urban mobility planning [12]. On-demand transport services have significant potential to enhance urban mobility by providing flexible and efficient alternatives to traditional fixed-route public transportation Techniques such as optimal control, genetic algorithms, and experiential optimization methods are increasingly applied to enhance braking strategies and safe headway control. Intelligent Transportation Systems (ITS) play a crucial role in developing sustainable urban environments by improving traffic efficiency, safety, and overall transportation management. Hybrid AI approaches, such as combining transfer learning with local search, have been applied to optimize vehicle routing problems, further advancing efficiency and sustainability in urban transportation systems [13–15]. As brainy and autonomous vehicles become more prevalent, the integration of real-time sensing, predictive analytics, and automated control systems introduces new challenges and opportunities in the prevention of rear-end collision. Advances in digital human modeling contribute significantly to the analysis and design of human-centered systems by integrating computational modeling with ergonomic and behavioral insights [16]. Emerging technologies for counting electric vehicles and connected autonomous vehicles, require refined dynamic models capable of representing varied traffic environments [17]. Hybrid modeling approaches that combine physics-based collision dynamics with machine learning techniques are gaining attention for improving system reliability and safety performance. AI-driven methods are enhancing urban public transportation by improving efficiency and sustainability through optimized intersections [18, 19]. Despite significant advances in collision modelling and prevention strategies, several challenges remain. Real-time scheduling optimization is essential for autonomous public transport systems to effectively respond to dynamic booking demands and improve service efficiency [20]. Furthermore, ensuring model robustness under uncertain traffic conditions and diverse driver behaviors is critical for practical implementation. Artificial intelligence techniques are increasingly used for demand forecasting and route optimization in public transportation systems, particularly in large metropolitan areas. Dynamic trip-vehicle assignment for on-demand high-capacity ride-sharing illustrates how AI can optimize urban mobility and improve sustainability. Understanding consumer preferences is essential for designing efficient and sustainable urban public transportation systems [21–23]. Recent studies have increasingly applied fuzzy logic based approaches to simulate real-world traffic situations by considering heterogeneous driver behaviors and uncertainty in decision-making processes. Such models aim to enhance traffic safety and efficiency by minimizing waiting time, reducing queue length, and improving overall traffic stability. Chai et al. [4] proposed a simulation-based approach to measure drivers' cognitive failures via a combination of fuzzy logic and cellular automata modeling techniques. Azimirad and Haddadnia [24] developed a novel fuzzy traffic controller to formulate and optimize signal control strategies at isolated signalized intersections. An et al. [25] introduced a dynamic fuzzy neural network model for the prediction of traffic flow, thus enabling accurate forecasting under chaotic traffic conditions. Most recently, Almadi et al. [26] has proposed an adaptive fuzzy pattern classification framework to simulate nonlinear and multi-dimensional transition processes, particularly for identifying lane-changing intentions among a diverse type of drivers.

This study represents one of the latest contributions in fuzzy-based traffic modeling by integrating adaptive pattern recognition with driver behavioral analysis. Despite these advancements, existing fuzzy-based models primarily focused on traffic flow control, prediction, and lane-changing behavior, with limited attention devoted to integrating fuzzy behavioral modeling into two-vehicle rear-end collision dynamics [27]. Since rear-end collisions are strongly influenced by uncertainties in perception-reaction time, braking intensity, and car-following behavior, incorporating fuzzy inference mechanisms into collision dynamics modeling more realistically represent the occurrence and severity of crashes. Therefore, extending classical mechanical collision models with fuzzy logic–based behavioral

components forms the central motivation of the present study. In conclusion, mathematical modeling of two-vehicle rear-end collisions is fundamental for understanding crash dynamics, improving vehicle safety systems, and enhancing urban traffic management. As transportation systems evolve toward automation and connectivity, the development of integrated, data-driven, and dynamic modeling frameworks will be essential for reducing collision frequency and improving overall roadway safety.

2 Model Formulation for the Proposed Model

In the next section, we present the mathematical formulation of the model, which divide the whole system into five classes: A is used for the position of Vehicle "A", which has constant velocity. B is used for the position of Vehicle "B", C is collision-phase vehicles, D is the distance between Vehicles "A" and "B", and S is separated vehicles. Where $d_0 > \frac{V_1 - V_2}{\delta \text{ B}}$ and $\triangle VA(t) = V_1 - V_2$, the remaining parameters are discussed in Table 1. The system of equations governing the rear-end collision model is as follows:

$$\begin{cases} \frac{dA}{dt} = \Omega - \frac{\beta_0}{d_0}\Delta VA - vA, \\ \frac{dB}{dt} = \frac{\beta_0}{d_0}\Delta VA - (\delta + v)B, \\ \frac{dC}{dt} = \delta B - (\omega + v)C, \\ \frac{dD}{dt} = \omega C - (\varrho + v)D, \\ \frac{dS}{dt} = \varrho D - vS. \end{cases} \tag{1}$$

with initial conditions: $A(0) = A_0 \geq 0, \quad B(0) = B_0 \geq 0, \quad C(0) = C_0 \geq 0, \quad D(0) = D_0 \geq 0, \quad S(0) = S_0 \geq 0.$

Table 1. Parameters and descriptions for collision dynamics

Parameter	Description	Unit
Ω	Traffic inflow rate	vehicles/time
β_0	Baseline interaction coefficient	1/(velocity time)
d_0	Initial distance between Vehicle A and Vehicle B	m
$t_{\text{collision}}$	Time at which the collision occurs, if any	seconds
δ	Braking-to-collision rate	1/time
ω	Collision-to-damage rate	1/time
ϱ	Clearance rate	1/time
v	Speed of the lead vehicle, Vehicle A	1/time
V_1	Rear vehicle speed	m/s
V_2	Front vehicle speed	m/s

3 Theoretical Analysis of the Proposed Model

3.1 Positivity and Boundedness Analysis

By taking these properties into justification, it can be assured that model is both feasible and realistic, hence providing valuable insights into the system dynamics. To analyze the model, we present some important properties, which concern the feasibility of the model.

Theorem 1: If the initial conditions of the model equations are non-negative $A(0) > 0, B(0) > 0, C(0) > 0, D(0) > 0, S(0) > 0$, then the solutions at any time t are also non-negative. That is, $A(\text{t}) > 0, B(\text{t}) > 0, C(\text{t}) > 0, D(\text{t}) > 0$ and $S(\text{t}) > 0$, for all $t \geq 0$.

Proof: To show the proposed model positive invariant, we consider the first equation of model:

$$\frac{\text{d(t)A}}{\text{dt}} = \Omega - \frac{\beta_0}{\text{d}_0}\Delta\text{VA(t)} - v\ \text{A(t)} \tag{2}$$

Since $\Omega > 0$, then Eq. (2) can be written as

$$\frac{\text{d(t)A}}{\text{dt}} \geq -\left(\frac{\beta_0}{\text{d}_0}\Delta\ \text{V} - \text{v}\right)\text{A(t)} \tag{3}$$

$$\frac{\text{d(t)A}}{\text{dt}} \geq -k_1\ \text{A(t)} \Rightarrow k_1 = \left(\frac{\beta_0}{\text{d}_0}\Delta\ \text{V} - v\right) \tag{4}$$

Now using the basic method of integration, variable separable method and simplify Eq. (4),

$$\frac{1}{\mathrm{A(t)}}\frac{\mathrm{d(t)A}}{\mathrm{dt}} \geq -k_1 \Rightarrow \frac{1}{\mathrm{A(t)}}\mathrm{d(t)A} \geq -k_1\mathrm{dt} \tag{5}$$

Applying integration on both sides of Eq. (5), we get

$$\int_{\mathrm{A_0}}^{\mathrm{A(t)}} \frac{1}{\mathrm{A(t)}}\mathrm{A\ d(t)} \geq -k_1 \int_0^t \mathrm{dA} \tag{6}$$

$$\ln\ \mathrm{A(t)} - \ln \mathrm{A_0} \geq -k_1\mathrm{t} \Rightarrow \ln\left(\frac{\mathrm{A(t)}}{\mathrm{A_0}}\right) \geq -k_1\mathrm{t} \tag{7}$$

$$\frac{\mathrm{A(t)}}{\mathrm{A_0}} \geq \mathrm{e^{-kt}} \Rightarrow\ \mathrm{A(t)} \geq \mathrm{A_0 e^{-kt}} \tag{8}$$

Re substitution, the value of $k_1 = \left(\frac{\beta_0}{\mathrm{d_0}}\Delta\ \mathrm{V} - v\right)$ in Eq. (6), we obtain

$$A(t) \geq A_0 \exp\left[\left(\frac{\beta_0}{d_0}\Delta V - v\right)t\right] > 0 \tag{9}$$

From Eq. (7), as the exponential function is always positive and $\mathrm{A_0} \geq 0$, so $\mathrm{A}(t) > 0$ for all $t > 0$, it shows that $\mathrm{A}(t) > 0$ is positive invariant. By similar way, we can also show that $B(t) > 0, C(\mathrm{t}) > 0, D(t) > 0$ and $S(t) > 0$, for all $t \geq 0$.

Theorem 2: All solutions of the model equations are uniformly bounded and remain within a feasible region for all $t \geq 0$.

Proof: Let consider that $\Sigma = \left\{\mathrm{A}(t), \mathrm{B}(t), \mathrm{C}(t), \mathrm{D}(t), \mathrm{S(t)} \in \mathrm{R}^5/0 \leq \mathrm{N}(t) \leq \frac{\Omega}{\mathrm{v}}\right\}$

Is the positive set, and the rate of change of the total population of cars is given by:

$$\frac{dN}{dt} = \frac{dA(t)}{dt} + \frac{dB(t)}{dt} + \frac{dC(t)}{dt} + \frac{dD(t)}{dt} + \frac{dS(t)}{dt} = \Omega - vN \tag{10}$$

$$\frac{dN}{dt} = \Omega - vN \tag{11}$$

To show that $N(t)$ is bounded, we solve the ordinary differential Eq. (9) since $\Omega > 0$, and rearranging Eq. (9), we get:

$$\frac{dN}{dt} \geq -vN = \ln N \geq -k_2\mathrm{t} + C_2 \tag{12}$$

where, C_2 is a constant of integration, applying the initial condition $N(0) = N_0$, in Eq. (10) we obtain:

$$N(t) = N_0\mathrm{e}^{-k_2\mathrm{t}} \Rightarrow N(t) \geq N_0\mathrm{e}^{-k_2\mathrm{t}} \tag{13}$$

It is clear from Eq. (11) $N_0 \geq 0$ and $\mathrm{e}^{-k_2\mathrm{t}} \geq 0$, so $N(t) \geq 0$ for all $t \geq 0$, it shows that the function is bounded above, now to show that the function is bounded below, as $t \geq 0$ and $k_2 \geq 0$ but $-k_2 t \leq 0$ and the exponential function is increasing, so $\mathrm{e}^{-k_2\mathrm{t}} \leq \mathrm{e}^0 = 1$. Now multiply both sides by $N_0 > 0$, we get $N_0\mathrm{e}^{-k_2\mathrm{t}} \leq N_0$, thus $N(t) \leq N_0$, this property shows that the function is bounded above. Combine the inequalities $N(t) \geq 0$ and $N(t) \leq N_0$, we obtain $0 \leq N(t) \leq N_0$; from this relation, the function is bounded above and bounded below, so it is bounded.

Figure 1 illustrates the dynamics of the total population $N(t)$ over time to show its bounded behavior. The graph illustrates the contributions of each compartment $(A(t), B(t), C(t), D(t)$ and $S(t))$) to the total population of the cars, to demonstrate the constraints $N_0e^{-kt} \leq N(t) \leq N_0e^{kt}$ for $t \geq 0$.

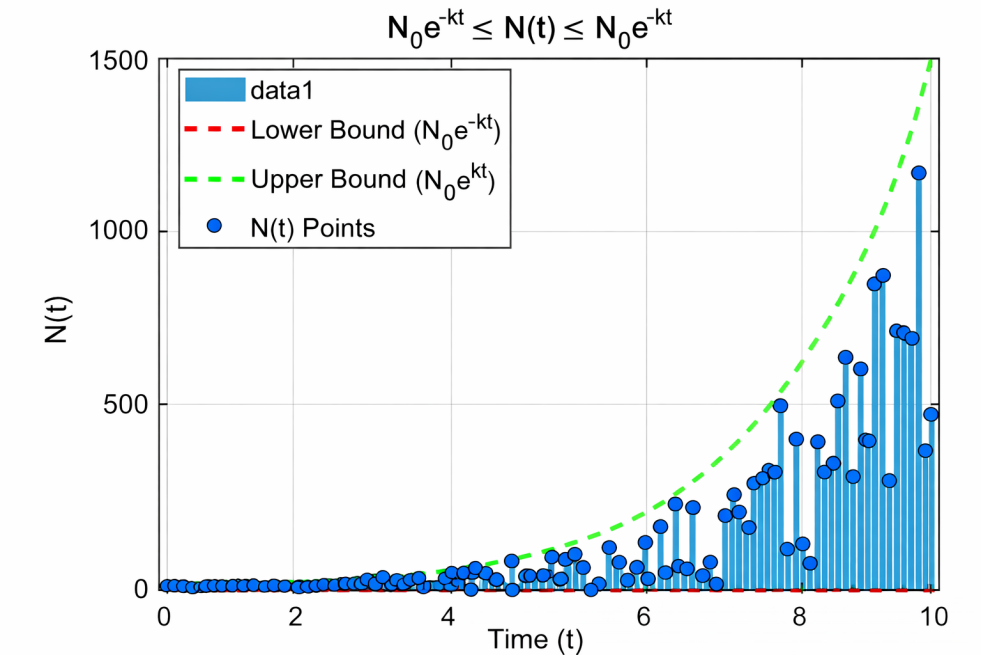

Figure 1. Dynamics of the total population N(t) over time to show its bounded behavior

4 Threshold Parameter $\mathcal{R}_0$ and Equilibrium Points

For the rear-end collision model, $\mathcal{R}_0$ can be interpreted as a threshold number, representing the ratio of the required stopping distance of the following vehicle to the available initial spacing, based on the parameters such as speeds, distance, and deceleration. If $\mathcal{R}_0$ is greater than a certain threshold which can depend on the initial gap d_0, the likelihood of a collision increases, i.e., $\mathcal{R}_0 > 1$ and if $\mathcal{R}_0$ is below this threshold, then the vehicles are far apart enough and the deceleration of Vehicle B is high enough that a collision is avoided, i.e., $\mathcal{R}_0 \leq 1$. The threshold number for the proposed model (Eq. (1)) is given by:

$$\mathcal{F} = \begin{pmatrix} \frac{\beta_0}{d_0}\Delta V A \\ \vdots \\ 0 \\ 0 \\ \vdots \end{pmatrix}, \quad \mathcal{V} = \begin{pmatrix} (\delta + v)B \\ (\omega + v)\mathbb{C} - \delta B \\ \vdots \\ (\varrho D - vS) - \omega C \\ \vdots \end{pmatrix} \tag{14}$$

$$\mathcal{F}' = \left.\frac{\partial \mathcal{F}}{\partial x_i}\right|_{E_0} = \begin{pmatrix} 0 & \frac{\beta_0}{d_0}\Delta V A & 0 & 0 & \vdots \\ 0 & 0 & \vdots & 0 & \vdots \\ \vdots & \vdots & \vdots & \vdots & \vdots \\ \vdots & 0 & 0 & \vdots & \vdots \end{pmatrix}, \mathcal{V}' = \left.\frac{\partial \sqsubseteq_i}{\partial x_i}\right|_{E_0} = \begin{pmatrix} \delta + v & \vdots & 0 & 0 & 0 \\ 0 & \vdots & 0 & 0 & 0 \\ \vdots & \vdots & \vdots & \vdots & \vdots \\ \vdots & \vdots & \vdots & \vdots & \vdots \\ 0 & \vdots & \omega + v & \varrho - v & 0 \end{pmatrix} \tag{15}$$

$$(\mathcal{V}')^{-1} = \begin{pmatrix} \frac{1}{\delta+v} & 0 & 0 \\ \frac{\delta}{(\delta+v)(\omega+v)} & \frac{1}{\delta+v} & 0 \\ \vdots & \vdots & \vdots \; \vdots \; \vdots \\ \frac{\delta\omega}{(\delta+v)(\omega+v)(\varrho-v)} & \frac{\delta\omega}{(\delta+v)(\omega+v)(\varrho-v)} & \vdots \; 0 \; \vdots \\ 0 & 0 & \vdots \; 0 \; \vdots \end{pmatrix} \tag{16}$$

Now calculate $\mathcal{R}_0$, we use the next generation matrix defined as,

$$\mathcal{F}' \cdot (\mathcal{V}')^{-1} = \begin{pmatrix} 0 & \frac{\beta_0}{d_0}\Delta V A & \vdots & 0 & \vdots \\ 0 & 0 & \vdots & 0 & \vdots \\ \vdots & \vdots & \vdots & \vdots & \vdots \\ \vdots & \vdots & \vdots & \vdots & \vdots \\ 0 & 0 & \vdots & 0 & \vdots \end{pmatrix} \begin{pmatrix} \frac{1}{\delta+v} & 0 & \vdots & 0 & \vdots \\ \frac{\delta}{(\delta+v)(\omega+v)} & \frac{1}{\delta+v} & \vdots & 0 & \vdots \\ \vdots & \vdots & \vdots & \vdots & \vdots \\ \frac{\delta\omega}{(\delta+v)(\omega+v)(\varrho-v)} & \frac{\delta\omega}{(\delta+v)(\omega+v)(\varrho-v)} & \vdots & 0 & \vdots \\ 0 & 0 & \vdots & 0 & \vdots \end{pmatrix} \tag{17}$$

The maximum eigenvalue of $\mathcal{F}' \cdot (\mathcal{V}')^{-1}$ is called the threshold number, which is given by:

$$\mathcal{R}_0 = \frac{\beta_0 \triangle V A \Omega \delta}{d_0 v(\delta + v)(\omega + v)} \tag{18}$$

4.1 Graphical Result

Figure 2 illustrates the effects of different parameters on the basic reproduction number $\mathcal{R}_0$, Figure 2a show the effect of Ω and β_0 on $\mathcal{R}_0$, Figure 2b effect of δ and V on $\mathcal{R}_0$, Figure 2c show the influence of ΔV and ω on $\mathcal{R}_0$ and d_0, v represents the effect on $\mathcal{R}_0$.

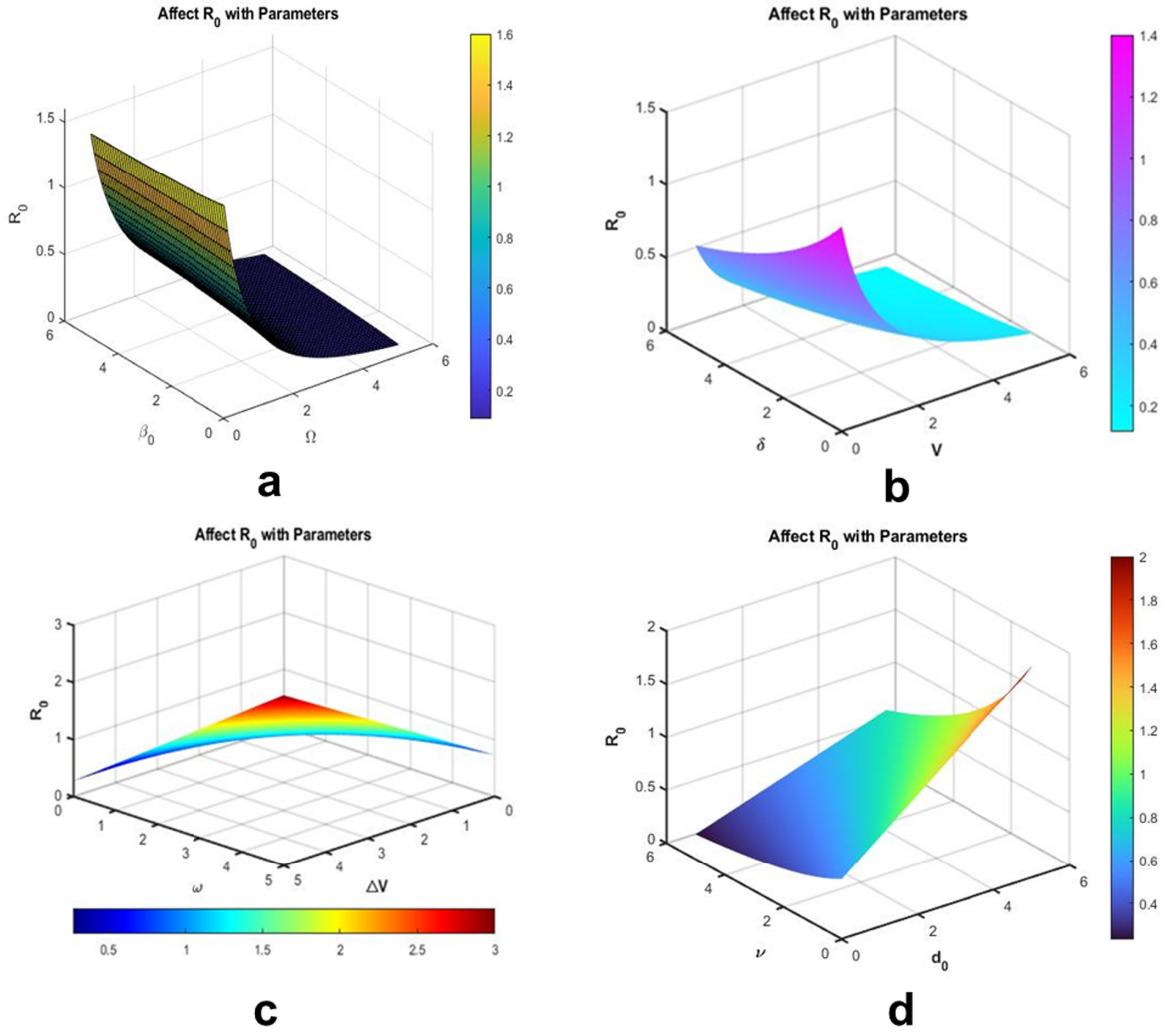

Figure 2. Effects of different parameters on the basic reproduction number $\mathcal{R}_0$

5 Stability Analysis of the Proposed Model

5.1 Local Stability Analysis

To study stability, we linearize the system at the equilibrium point by computing the Jacobin matrix of the system. The Jacobin matrix **J** describes how small changes in the state variables affect the time derivatives of the state variables. The Jacobin matrix is computed as follows:

$$\mathbf{J} = \begin{pmatrix} \frac{\partial f_1}{\partial A} & \frac{\partial f_1}{\partial B} & \frac{\partial f_1}{\partial C} & \frac{\partial f_1}{\partial D} & \frac{\partial f_1}{\partial S} \\ \frac{\partial f_2}{\partial A} & \frac{\partial 2}{\partial B} & \frac{\partial f_2}{\partial C} & \frac{\partial f_2}{\partial D} & \frac{\partial f_2}{\partial S} \\ \frac{\partial f_3}{\partial A} & \frac{\partial f_3}{\partial B} & \frac{\partial f_3}{\partial C} & \frac{\partial f_3}{\partial D} & \frac{\partial f_3}{\partial S} \\ \frac{\partial f_4}{\partial A} & \frac{\partial f_4}{\partial B} & \frac{\partial f_4}{\partial C} & \frac{\partial f_4}{\partial D} & \frac{\partial f_4}{\partial S} \\ \frac{\partial f_5}{\partial A} & \frac{\partial f_5}{\partial B} & \frac{\partial f_5}{\partial C} & \frac{\partial f_5}{\partial D} & \frac{\partial f_5}{\partial S} \end{pmatrix} \tag{19}$$

where, $f_1 = \Omega - \frac{\beta_0}{d_0}\Delta VA - vA$, $f_2 = \frac{\beta_0}{d_0}\Delta VA - (\delta + v)B$, $f_3 = \delta B - (\omega + v)C$, $f_4 = \omega C \quad (\varrho + v)D$, $f_5 = \varrho D - vS$.

So the Jacobin matrix (Eq. (19)) can be written as:

$$\mathbf{J} = \begin{pmatrix} -\frac{\beta_0}{d_0}\triangle VA & 0 & 0 & 0 & 0 \\ -\frac{\beta_0}{d_0}\triangle & -(\delta + v) & 0 & 0 & 0 \\ 0 & \delta & -(\omega + v) & 0 & 0 \\ 0 & 0 & \omega & (\varrho + v) & 0 \\ 0 & 0 & 0 & \varrho & -v \end{pmatrix} \tag{20}$$

To determine the stability of the system, we use the eigenvalue approaches. The eigenvalues of the matrix **J** are found by solving the characteristic equation, so Eq. (20) can be expressed as,

$$\det|\mathbf{J} - \boldsymbol{\lambda}\mathbf{I}| = \begin{pmatrix} -\frac{\beta_0}{d_0}\Delta VA - \lambda & 0 & 0 & 0 & 0 \\ -\frac{\beta_0}{d_0}\Delta & -(\delta + v) - \lambda & 0 & 0 & 0 \\ 0 & \delta & -(\omega + v) - \lambda & 0 & 0 \\ 0 & 0 & \omega & -(\varrho + v) - \lambda & 0 \\ 0 & 0 & 0 & \varrho & -v - \lambda \end{pmatrix} \tag{21}$$

where, $\lambda_1 = -\frac{\beta_0}{d_0}\Delta VA$, $\lambda_2 = -(\delta + v)$, $\lambda_3 = -(\omega + v)$, $\lambda_4 = -(\varrho + v)$, $\lambda_5 = -v$.

After some simplification, the matrix (Eq. (17)) is lower triangular and all the eigenvalues are the diagonal entries. And all eigenvalues are strictly negative. The equilibrium point is locally asymptotically stable.

5.2 Global Asymptotic Stability Analysis

In this part, we shall determine the Global Sensitivity Analysis (GSA) of model (Eq. (1)), at the points as follows:

$$E^0 = \left\{ \frac{\Omega}{\frac{\beta_0}{d_0}\triangle VA}, \frac{\frac{\beta_0}{d_0}\triangle VA}{(\delta + v)}, \frac{(\omega + v)}{(\delta + v)}, 0, \frac{\varrho}{v} \right\} \tag{22}$$

We shall use a Lyapunov function to analyze the system further.

Theorem 3: Model (1) is considered to be globally asymptotically stable (GAS) at the equilibrium where the threshold number $\boldsymbol{\mathcal{R}_0} \leq 1$ if $A = A_0$ and $D = D_0$, the system is not stable for $\mathcal{R}_0 > 1$.

Proof: By showing that the system is GAS, we have to show that $\mathcal{R}_0 \leq 1$ by using the following Lyapunov function technics, for this let suppose that:

$$\mathcal{H}(ABCDS) = \frac{1}{2}\left[((A - A_0) + (B - B_0) + (C - C_0) + (D - D_0) + (S - S_0))\right]^2 \tag{23}$$

To compute the time derivative of H, we need

$$\frac{d}{dt}\left((A - A_0) + (B - B_0) + (C - C_0) + (D - D_0) + (S - S_0)\right)^2 \tag{24}$$

Eq. (24) can be written as

$$\frac{d}{dt}(\,\mathrm{A} + \mathrm{B} + \mathrm{C} + \mathrm{D} + \mathrm{S}) - (\mathrm{A}_0 + \mathrm{B}_0 + \mathrm{C}_0 + \mathrm{D}_0 + \mathrm{S}_0) = \frac{d\,\mathrm{A}}{dt} + \frac{d\,\mathrm{B}}{dt} + \frac{d\mathrm{C}}{dt} + \frac{d\mathrm{D}}{dt} + \frac{d\,\mathrm{S}}{dt} \tag{25}$$

Substituting the model equations from Eq. (21), we get:

$$\frac{d}{dt}(\,\mathrm{A}+\mathrm{B}+\mathrm{C}+\mathrm{D}+\mathrm{S}) = (\mathcal{P}-\mathcal{Q}) \tag{26}$$

where, $\mathcal{P}$ are the positive parameters and $\mathcal{Q}$ are the negative parameters of the model, if $\mathcal{P} > \mathcal{Q}$ then $\frac{d\mathcal{H}}{dt} = (\mathcal{P}-Q)^{dt} < 0$. Thus, $\frac{d\mathcal{H}}{dt} < 0$ when $\mathcal{R}_0 \leq 1$, so $\mathcal{H}$ shows that it decreases function over time t which clearly indicates that the proposed model is GAS at the equilibrium point E^0.

Theorem 4: The proposed model is GAS at the equilibrium point if $R_0 > 1$.

Proof: To show that the model is GAS, we will consider the following Lyapunov function:

$$\mathcal{G}\,(y_1, y_2, \ldots, y_n) = \frac{1}{2}\sum_{i=1}^{n}(y_i - y_i^*)^2 \tag{27}$$

where, $y_i = (\mathrm{A}, \mathrm{B}, \mathrm{C}, \mathrm{D}, \mathrm{S})$ and $y_i^* = (\mathrm{A}^*,\ \mathrm{B}^*, \mathrm{C}^*, \mathrm{D}^*,\ \mathrm{S}^*)$.

First, we compute the time derivative of $\mathcal{G}$:

$$\frac{dG}{dt} = \sum_{i=1}^{n}(y_i - y_i^*)\,\frac{dy_i}{dt} \tag{28}$$

$$\frac{dG}{dt} = \left((A-A_0)\,\frac{dA}{dt} + (B-B_0)\,\frac{dB}{dt} + (C-C_0)\,\frac{dC}{dt} + (D-D_0)\,\frac{dD}{dt} + (S-S_0)\,\frac{dS}{dt}\right) \tag{29}$$

Let $\frac{dN}{dt} = (\mathrm{A}+\mathrm{B}+\mathrm{C}+\mathrm{D}+\mathrm{S})$ and suppose $\frac{dG}{dt} = [N(t) - (\mathrm{A}^*+\mathrm{B}^*+\mathrm{C}^*+\mathrm{D}^*+\mathrm{S}^*)]\,\frac{dG}{dt}$, We obtain

$$\frac{dG}{dt} = (\mathrm{A}+\mathrm{B}+\mathrm{C}+\mathrm{D}+\mathrm{S}) = \frac{\Omega - \delta \mathrm{C}^*}{(\varrho + v)} \tag{30}$$

$$\frac{dG}{dt} = [(\mathrm{A}^*+\mathrm{B}^*+\mathrm{C}^*+\mathrm{D}^*+\mathrm{S}^*)] = \frac{\Omega - \delta \mathrm{D}^*)}{(\varrho + v)} \tag{31}$$

Thus, we can conclude the following:

$$\frac{dG}{dt} = \left|N(t) - \frac{\Omega - \delta \mathrm{C}^*}{(\varrho + v)}\right| \left|-\delta N(t) - \frac{\Omega - \delta \mathrm{C}^*}{(\varrho + v)}\right| \tag{32}$$

Hence, the Eq. (32) can be written as:

$$\frac{dG}{dt} = -\delta \left|N(t) - \frac{\Omega - \delta \mathrm{C}^*}{(\varrho + v)}\right|^2 < 0 \tag{33}$$

Since $\frac{dG}{dt} < 0$ which means that the function is decreasing and satisfied all the conditions of Lyapunov function, so the system is GAS.

6 Sensitivity Analysis of the Model

Sensitivity analysis of the key safety indicators, such as relative impact velocity or minimum safe headway distance with respect to the model parameters, is very important for the present study. It enables us to identify the most influential parameters that play a significant role in the occurrence and severity of rear-end collision. These parameters typically include vehicle speed, drivers' reaction time, braking deceleration, headway distance, road friction coefficient, and vehicle mass. In this section, the sensitivity of various key parameters of the rear-end collision dynamics model was carried out to determine their relative influence on collision risk and impact severity. The sensitivity of the basic reproductive number R_0 with respect to a parameter η is given by:

$$\gamma_{\xi}^{R_0} = \frac{\partial R_0}{\partial \xi} \times \frac{\xi}{R_0} \tag{34}$$

where, ξ can be any of the parameters in the set:

$$\xi \in \{\Omega, \beta_0, \Delta V, \delta, d_0, v, \omega, \} \tag{35}$$

$$\frac{\partial \mathcal{R}_0}{\partial \Omega} \times \frac{\Omega}{\mathcal{R}_0} = \frac{1}{\partial \Omega}\left(\frac{\beta_0 \triangle V A \Omega \delta}{d_0 v(\delta+v)(\omega+v)}\right) \times \frac{\lambda}{\frac{\beta_0 \triangle V A \Omega \delta}{d_0 v(\delta+v)(\omega+v)}} \approx 1 \tag{36}$$

$$\frac{\partial R_0}{\partial \delta} \times \frac{\delta}{\mathcal{R}_0} = \frac{1}{\partial \delta}\left(\frac{\beta_0 \triangle V A \Omega \delta}{d_0 v(\delta+v)(\omega+v)}\right) \times \frac{\delta}{\frac{\beta_0 \triangle V A \Omega \delta}{d_0 v(\delta+v)(\omega+v)}} \approx 0.132 \tag{37}$$

$$\frac{\partial R_0}{\partial \beta_0} \times \frac{\beta_0}{\mathcal{R}_0} = \frac{1}{\partial \beta_0}\left(\frac{\beta_0 \Delta V A \Omega \delta}{d_0 v(\delta+v)(\omega+v)}\right) \times \frac{\beta_0}{\beta_0 \Delta V A \Omega \delta} \approx 0.423 \tag{38}$$

$$\frac{\partial R_0}{\partial d_0} \times \frac{d_0}{R_0} = \frac{1}{\partial d_0}\left(\frac{\beta_0 \triangle V A \Omega \delta}{d_0 v(\delta+v)(\omega+v)}\right) \times \frac{d_0}{\frac{\beta_0 \triangle V A \Omega \delta}{d_0 v(\delta+v)(\omega+v)}} \approx -0.0035 \tag{39}$$

$$\frac{\partial R_0}{\partial v} \times \frac{v}{R_0} = \frac{1}{\partial v}\left(\frac{\beta_0 \triangle V A \Omega \delta}{d_0 v(\delta+v)(\omega+v)}\right) \times \frac{v}{\frac{\beta_0 \triangle V A \Omega \delta}{d_0 v(\delta+v)(\omega+v)}} \approx -0.0896 \tag{40}$$

Sensitivity Analysis of R_0 with respect to the different parameters shows that Ω, δ, ω, and β_0 have a direct relationship with R_0, while the sensitivity index of R_0 with respect to d_0, v, and ΔV shows an inverse variation, as illustrated in Figure 3.

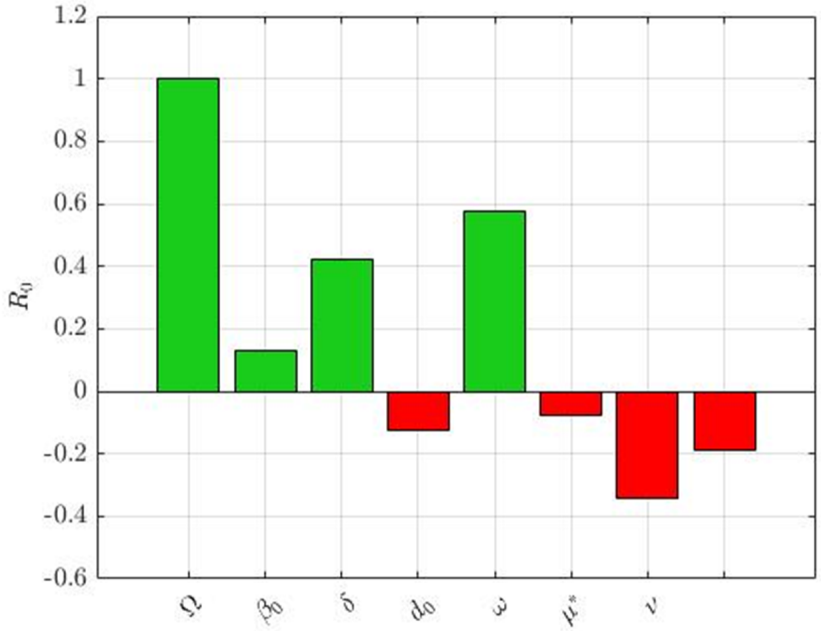

Figure 3. Sensitivity Analysis of R_0 with different parameters

7 Formulation of Optimal Control Problem

$$\begin{cases} \frac{dA}{dt} = \Omega - \frac{\beta_0}{d_0}\Delta V A - vA \cdot (1 - \mathfrak{U}_1^*(t)) \\ \frac{dB}{dt} = \frac{\beta_0}{d_0}\Delta V A - (\delta+v)B \cdot (1 - \mathfrak{U}_2^*(t)) \\ \frac{dC}{dt} = \delta B - (\omega+v)C \cdot (1 - \mathfrak{U}_3^*(t)) \\ \frac{dD}{dt} = \omega C - (\varrho+v)D \cdot (1 - \mathfrak{U}_4^*(t)) \\ \frac{dS}{dt} = \varrho D - vS \cdot (1 - \mathfrak{U}_5^*(t)) \end{cases} \tag{41}$$

With initial conditions: $A(0) = A_0 \geq 0, \quad B(0) = B_0 \geq 0, \quad C(0) = C_0 \geq 0, \quad D(0) = D_0 \geq 0, \quad S(0) = S_0 \geq 0$.

In order to reduce the road accidents rate, we define the objective functional to reduce and minimize the number of accidents while balancing intervention costs:

$$\mathbf{J}\left(\mathfrak{U}_1^*(t),\mathfrak{U}_2^*(t),\mathfrak{U}_3^*(t),\mathfrak{U}_4^*(t),\mathfrak{U}_5^*(t)\right)=\int_0^{T_f}\Big(\mathcal{C}_1^*(A(t))+\mathcal{C}_2^*+\mathcal{C}_3^*+\mathcal{C}_4^*+\frac{1}{2}\left(\mathcal{C}_5^*\mathfrak{U}_1^*(t)+\mathcal{C}_6^*\mathfrak{U}_3^*(t)\right.$$
$$\left.+\mathcal{C}_7^*\mathfrak{U}_4^*(t)+\mathcal{C}_7^*\mathfrak{U}_5^*(t)\right)\Big)\,dt \tag{42}$$

In Eq. (42), $A(t)$ is the number (or probability) of rear-end collisions at time t, $\mathfrak{U}_1^*(t)$ is braking control, $\mathfrak{U}_2^*(t)$ is ACC intervention, $\mathfrak{U}_3^*(t)$ is warning system activation and $\mathfrak{U}_4^*(t)$ is the driver response enhancement control. $\mathcal{C}_m^*>0,\ \mathrm{m}=1,2,3,4,5$ represents balancing cost factors and T_f shows the final time.

7.1 Existence of the Optimal Control Problem

In this section, we prove the existence of the control problem. We define the Hamiltonian $\widehat{H}$ for the optimal control problem as follows:

$$\widehat{\mathcal{H}}=\boldsymbol{L}\left(A(t),B(t),C(t),D(t),S(t),\mathfrak{U}_1^*(t),\mathfrak{U}_2^*(t),\mathfrak{U}_3^*(t),\mathfrak{U}_4^*(t),\mathfrak{U}_5^*(t)\right)$$
$$+\eta_1^*\frac{dA(t)}{dt}+\eta_3^*\frac{dB(t)}{dt}+\eta_3^*\frac{dC(t)}{dt}+\eta_4^*\frac{dD(t)}{dt}+\eta_5^*\frac{dS(t)}{dt} \tag{43}$$

Theorem 5: For control problem, there exists $\mathfrak{U}^*(t)=(\mathfrak{U}c_1^*(t),\mathfrak{U}_2^*(t),\mathfrak{U}_3^*(t),\mathfrak{U}_4^*(t),\mathfrak{U}_5^*(t))\in\boldsymbol{U}$ such that

$$\min_{\left(\mathfrak{U}c_1^*(t),\mathfrak{U}_2^*(t),\mathfrak{U}_3^*(t),\mathfrak{U}_4^*(t),\mathfrak{U}_5^*(t)\right)\in\boldsymbol{U}} J\left(\mathfrak{U}c_1^*(t),\mathfrak{U}_2^*(t),\mathfrak{U}_3^*(t),\mathfrak{U}_4^*(t),\mathfrak{U}_5^*(t)\right)=J\left(\mathfrak{U}c_1^*(t),\mathfrak{U}_2^*(t),\mathfrak{U}_3^*(t),\mathfrak{U}_4^*(t),\mathfrak{U}_5^*(t)\right) \tag{44}$$

To validate the existence and prevalence of optimal control, several analytical techniques were employed. First, all state variables and control variables are assumed to be non-negative, to ensure physical feasibility and mathematical consistency of the model. During the reduction of the problem, the required convexity of the objective functional with respect to the optimal controls $\mathfrak{U}c_1^*(t),\mathfrak{U}_2^*(t),\mathfrak{U}_3^*(t),\mathfrak{U}_4^*(t),\mathfrak{U}_5^*(t)$ is verified and satisfied. The admissible control set

$$\boldsymbol{U}=\{\mathfrak{U}c_1^*(t),\mathfrak{U}_2^*(t),\mathfrak{U}_3^*(t),\mathfrak{U}_4^*(t),\mathfrak{U}_5^*(t)\text{ for all }\mathfrak{U}_i^*\geq 0\} \tag{45}$$

is convex and closed by definition. This property plays a crucial role in establishing the existence of an optimal control pair. Because the control set is convex and closed, and the integrand is convex in the controls, the necessary conditions for the existence of an optimal control are satisfied. Consequently, the formulated optimal control system is well-posed and mathematically solid, which certifies the proof and validation of the optimal control framework.

Theorem 6: Let $\mathfrak{U}c_1^*(t),\mathfrak{U}_2^*(t),\mathfrak{U}_3^*(t),\mathfrak{U}_4^*(t),\mathfrak{U}_5^*(t)$ be the control variables and $\mathrm{A}^*,\ \mathrm{B}^*,\mathrm{C}^*,\ \mathrm{B}^*,\ \mathrm{S}$ be the solutions of the optimal control model, Eq. (42) then there exists adjoint variables $\eta_m^*(t)$, for $m=1,\ldots,5$, satisfying the following equations:

$$\frac{d\eta_1^*}{dt}=bA\left(\eta_1^*-\eta_2^*\right)+\left(\eta_1^*-\eta_3^*\right)\left(1-u_1^*(t)\right)+m\eta_1^* \tag{46}$$

$$\frac{d\eta_2^*}{dt}=-\mathcal{C}_1^*+\left(\eta_2^*-\eta_3^*\right)a_1+\left(\eta_2^*-\eta_3^*\right)\left(1-u_1^*(t)\right)+m\eta_2^* \tag{47}$$

$$\frac{d\eta_3^*}{dt}=-\mathcal{C}_2^*+\left(\eta_1^*-\eta_2^*\right)bS+\eta_3^*(m+g+r+h)+\left(\eta_3^*-\eta_4^*\right)\left(1-u_2^*(t)\right) \tag{48}$$

$$\frac{d\eta_4^*}{dt}=-\mathcal{C}_3^*+\eta_4^*(m+t+f+h)+\left(\eta_4^*-\eta_3^*\right)\left(1-u_2^*(t)\right)+\eta_3^*t+\eta_4^*f \tag{49}$$

Proof: Let suppose that $\mathrm{A}(t)=\mathrm{A}^*\ \mathrm{B}(t)=\mathrm{B}^*\mathrm{C}(t)=\mathrm{C}^*\mathrm{D}(t)=\mathrm{D}^*\ \mathrm{S}(t)=\mathrm{S}^*$ and differentiate the Hamiltonian with respect to state variables $\mathrm{A}(t),\mathrm{B}(t),\mathrm{C}(t),\mathrm{D}(t)$, and $\mathrm{S}(t)$, we get the following adjoint system:

$$\frac{d\eta_m^*(t)}{dt}=-\frac{\partial\mathcal{H}}{\partial x_m} \tag{50}$$

where, $\eta_m^*(t)$ represents the adjoint variables associated with the state variables $x_m(t) = \mathrm{A}(t), \mathrm{B}(t), \mathrm{C}(t), \mathrm{D}(t), \mathrm{S}(t)$. The transversal conditions are given by: $\eta_m^*(t)\,(T_f) = 0, m = 1, 2, \ldots, 5$, T_f is the final time.

Theorem 7: The control pairs $(\mathfrak{U}_1^*(t), \mathfrak{U}_2^*(t), \mathfrak{U}_3^*(t), \mathfrak{U}_4^*(t), \mathfrak{U}_5^*(t))$, which minimize the objective functional J over the region U, is given by:

$$\mathfrak{U}_1^*(t) = \min\left\{1, \max\left(\frac{(\eta_5^* - \eta_1^*)\,\mathcal{C} + (\eta_6^* - \eta_2^*)\,\mathrm{A}}{\mathcal{C}_1^*}, 0\right)\right\} \tag{51}$$

$$\mathfrak{U}_2^*(t) = \min\left\{1, \max\left(\frac{(\eta_6^* - \eta_3^*)\,\mathrm{F} + (\eta_6^* - \eta_5^*)\,\mathrm{B}}{\mathcal{C}_2}, 0\right)\right\} \tag{52}$$

$$\mathcal{U}_3^*(t) = \min\left\{1, \max\left(\frac{(\eta_6^* - \eta_1^*)\,\mathrm{C} + (\lambda_6^* - \eta_2^*)\,\mathrm{C}}{\mathcal{C}_3^*}, 0\right)\right\} \tag{53}$$

$$\mathfrak{U}_4^*(t) = \min\left\{1, \max\left(\frac{(\eta_6^* - \eta_3^*)\,\mathrm{F} + (\eta_6^* - \eta_5^*)\,\mathrm{S}}{\mathcal{C}_4}, 0\right)\right\} \tag{54}$$

Proof: By using the optimality condition, we get

$$\frac{\partial \mathcal{C}}{\partial \mathrm{u}_1} = \mathcal{C}_5^* \mathfrak{U}_1^*(\mathrm{t}) + (\eta_6^* - \eta_1^*)\,\mathrm{A} + (\eta_6^* - \eta_2^*)\,\mathrm{A} \tag{55}$$

$$\frac{\partial \mathcal{C}}{\partial \mathrm{u}_2} = \mathcal{C}_6 \mathfrak{U}_2^*(\mathrm{t}) + (\eta_3^* - \eta_6^*) + (\eta_5^* - \eta_6^*)\,\mathrm{C}, \frac{\partial \mathcal{C}}{\partial \mathfrak{U}_3} = \mathcal{C}_7 \mathfrak{U}_3(\mathrm{t}) + (\eta_4^* - \eta_6^*)\,\mathrm{B} \tag{56}$$

The optimal control variables $\mathfrak{U}_1^*(t), \mathfrak{U}_2^*(t), \mathfrak{U}_3^*(t)$, such that:

$$\mathfrak{U}_1^*(\mathrm{t}) = \frac{(\eta_6^* - \eta_1^*)\,\mathrm{C} + (\eta_6^* - \eta_2^*)\,\mathrm{C}}{\mathcal{C}_5^*} \tag{57}$$

$$\mathcal{U}_2^*(\mathrm{t}) = \frac{(\eta_6^* - 3)\,\mathrm{F} + (\eta_6^* - \eta_3^*)\,\mathrm{D}}{\mathcal{C}_6} \tag{58}$$

The property of the control space equations can be written as follows:

$$\mathfrak{U}_1^*(\mathrm{t}) = \begin{cases} 0 & \text{if} \quad \frac{(\eta_4^* - \eta_1^*)\mathcal{C} + (\eta_6^* - \eta_2^*)\mathrm{A}}{\mathcal{C}_3^*} \leq 0 \\ \frac{(\eta_6^* - \eta_1^*)\mathrm{C} + (\eta_4^* - \eta_2^*)D}{\mathcal{C}_3^*} & \text{if} \quad 0 < \frac{(\eta_4^* - \eta_1^*)\mathcal{C} + (\eta_4^* - \eta_2^*)\mathrm{B}}{\mathcal{C}_5^*} < 1 \\ 1 & \text{if} \quad \frac{(\eta_4^* - \eta_1^*)\mathrm{C} + (\eta_6^* - \eta_2^*)D}{\mathcal{C}_5^*} \geq 1 \end{cases} \tag{59}$$

$$\mathcal{U}_2^*(\mathrm{t}) = \begin{cases} 0 & \text{if} \quad \frac{(\eta_4^* - \eta_3^*)\mathbb{D} + (\eta_4^* - \eta_3^*)\mathrm{B}}{\mathcal{C}_4^*} \leq 0 \\ \frac{(\eta_4^* - \eta_3^*)\mathrm{T} + (\eta_4^* - \eta_3^*)\mathrm{C}}{\mathcal{C}_4^*} & \text{if} \quad 0 < \frac{(\eta_4^* - \eta_3^*)\mathrm{F} + (\eta_4^* - \eta_5^*)\mathrm{C}}{\mathcal{C}_4^*} < 1 \\ 1 & \text{if} \quad \frac{(\eta_6^* - \eta_3^*)\mathbb{C} + (\eta_4^* - \eta_5^*)D}{\mathcal{C}_4^*} \geq 1 \end{cases} \tag{60}$$

According to compact notation, $\mathfrak{U}_1^*(t), \mathfrak{U}_2^*(t), \mathfrak{U}_3^*(t)$ and $\mathfrak{U}_4^*(t)$ can be written as:

$$\mathfrak{U}_1^*(t) = \min\left\{1, \max\left(\frac{(\eta_4^* - \eta_1^*)\,A + (\eta_3^* - \eta_2^*)\,\mathrm{A}}{\mathcal{C}_3^*}, 0\right)\right\} \tag{61}$$

$$\mathfrak{U}_2^*(\mathrm{t}) = \min\left\{1, \max\left(\frac{(\eta_4^* - \eta_3^*)\,F + (\eta_4^* - \eta_3^*)\,\mathrm{B}}{\mathcal{C}_6}, 0\right)\right\} \tag{62}$$

$$\mathfrak{U}_3^*(t) = \min\left\{1, \max\left(\frac{(\eta_6^* - \eta_1^*)\,\mathrm{C} + (\eta_6^* - \eta_2^*)\,\mathrm{C}}{\mathcal{C}_3^*}, 0\right)\right\} \tag{63}$$

$$\mathfrak{U}_4^*(t) = \min\left\{1, \max\left(\frac{(\eta_6^* - \eta_3^*)\,\mathrm{F} + (\eta_6^* - \eta_5^*)\,\mathrm{S}}{\mathcal{C}_4}, 0\right)\right\} \tag{64}$$

8 Graphical Representation for the Rear-End Collision

The sequence of graphs in Figure 4 illustrates the progression of events in a rear-end collision scenario and the corresponding response of the control system. It shows how the system continuously monitors vehicle dynamics and detects a potential risk of collision. Once the risk is identified, the control mechanism activates warning or braking actions to reduce the possibility of a rear-end collision. As shown in the subsequent figures, the control system gradually stabilizes the vehicle behavior, maintains a safe following distance, and minimizes the likelihood or severity of collision. This sequence demonstrates the effectiveness of the proposed control strategy in preventing rear-end collisions and improving overall driving safety.

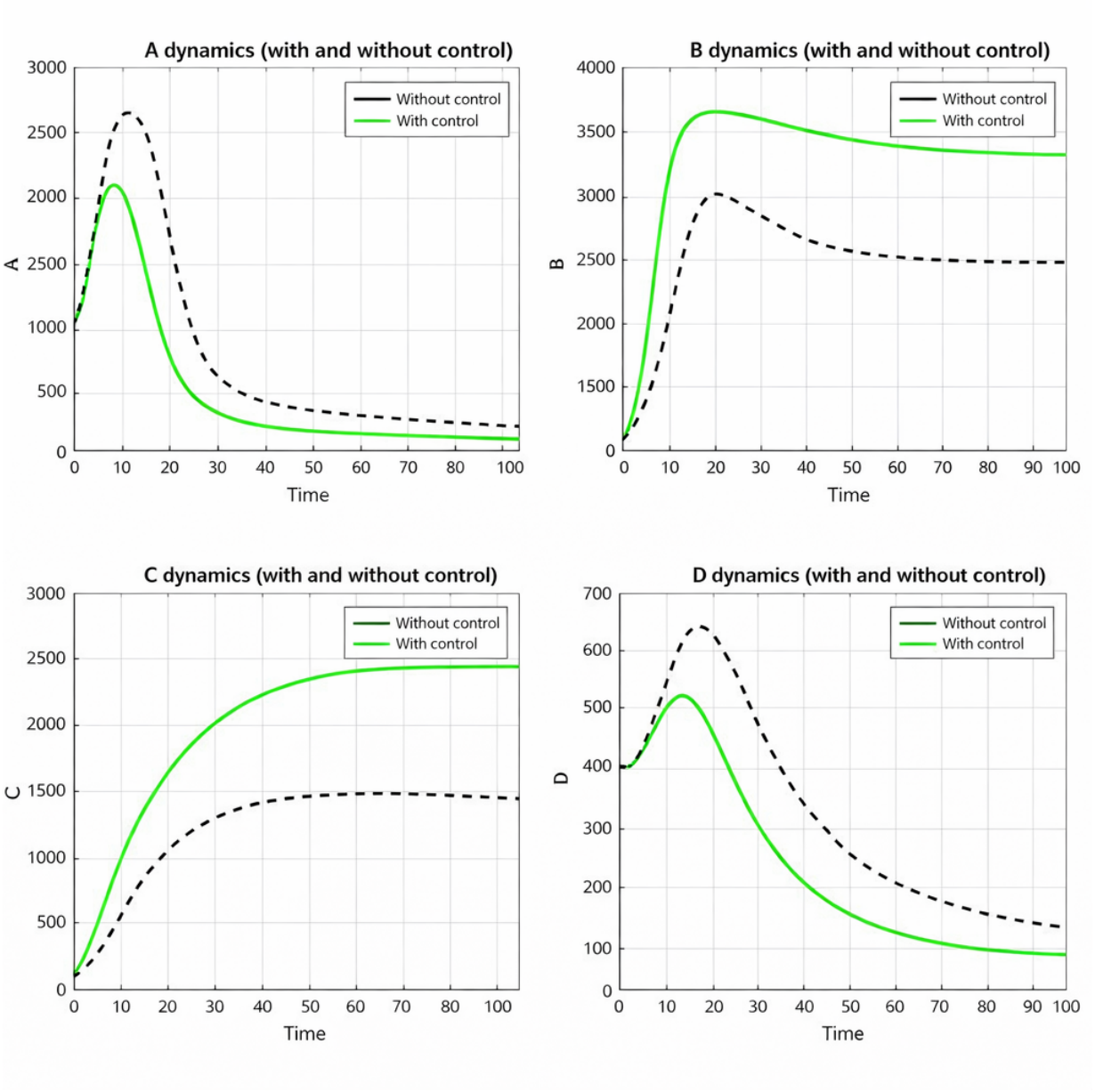

Figure 4. Sensitivity analysis of R_0 with different parameters

9 Numerical Simulation for the Proposed Model

In this study, we settled and implemented a numerical scheme to model the dynamics of the model by using various parametric values, as outlined in the associated table. By employing a system of ODEs and applying the Runge-Kutta 4th-order (RK4) method, we were able to simulate and analyze the evolution of different classes over time, such as the places of Vehicle A and Vehicle B, the relative distance between Vehicles A and B. For the numerical simulations, we used the parameters describe in the above Table 1 with the help of matlab software.

The simulation results of the rear-end collision scenario, shown in Figure 5, illustrate the time evolution of the positions of Vehicles A and B (Figure 5a) and (Figure 5b), the rear-end collision dynamics (Figure 5c), and the time evolution of the relative distance between the vehicles ((Figure 5d), highlighting the effectiveness of the control system in maintaining safe spacing.

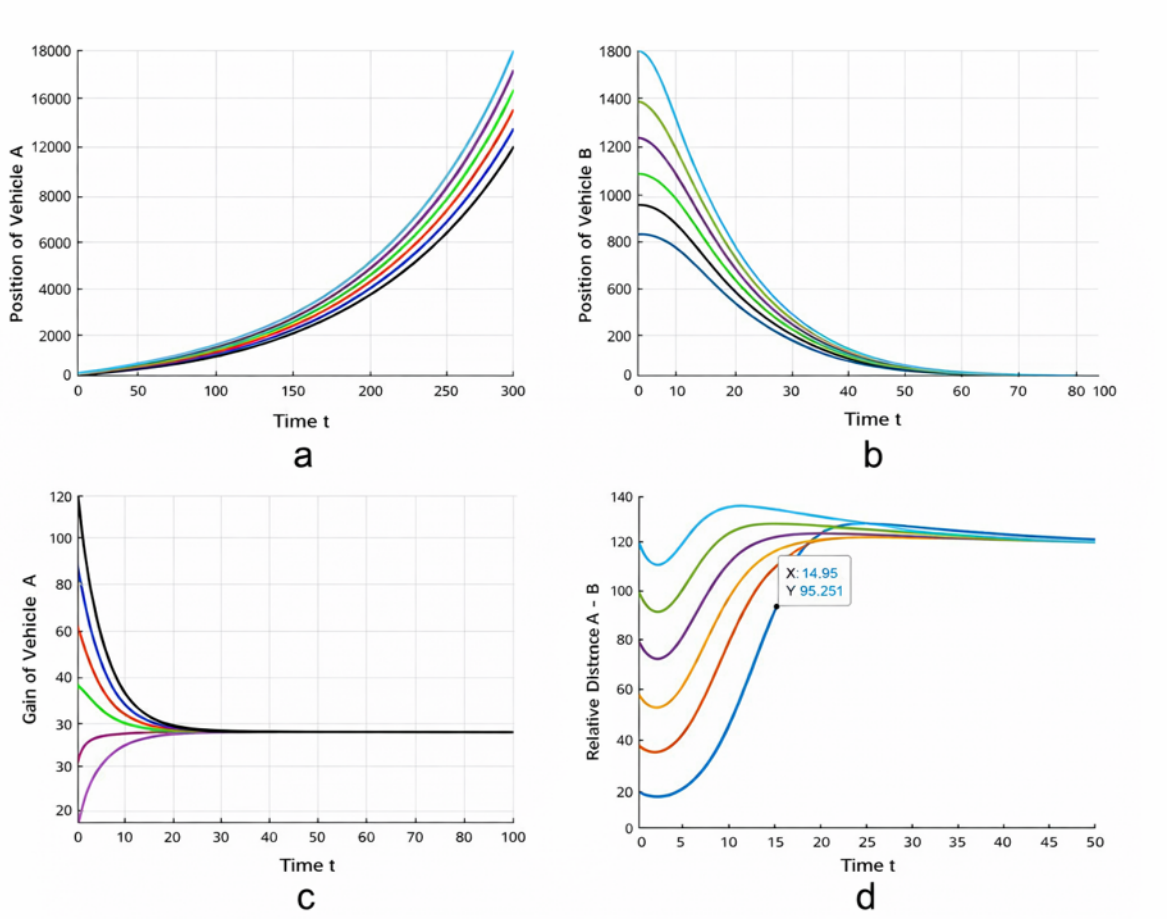

Figure 5. Simulation results illustrating the rear-end collision scenario

10 Conclusions

In conclusion, mathematical modeling and optimization techniques play an important role in reducing rear-end collisions and improving road safety. By using collision prediction models, calculations of braking distance, and data of real-time sensor, vehicles could better estimate safe following distances and react more effectively to sudden changes in traffic. The integration of machine learning and intelligent control systems further enhances accident prevention by adapting to driving patterns and traffic conditions. Overall, these advanced technologies contribute to safer roads, smoother traffic flow, and reduced accident-related losses.

Author Contributions

Conceptualization, W.U.R.; methodology and idea, M.A.; software, M.A.; validation, M.A., W.U.R., and Z.S.; formal analysis, M.A.; investigation, M.A.; resources, W.U.R.; data curation, M.A.; writing original draft preparation, M.A.; writing review and editing, M.A. and W.U.R.; visualization, Corresponding author: W.U.R. All authors have read and agreed to the published version of the manuscript.

Data Availability

The data used to support the findings of this study are available from the corresponding author upon request.

Conflicts of Interest

The authors declare no conflicts of interest.

References

[1] V. L. Vujadinovic, A. Damnjanovic, A. Cakic, D. R. Petkovic, M. Prelevic, V. Pantovic, M. Stojanovic, D. Vidojevic, D. Vranjes, and I. Bodolo, "AI-driven approach for enhancing sustainability in urban public transportation," *Sustainability*, vol. 16, no. 17, p. 7763, 2024. https://doi.org/10.3390/su16177763

[2] O. F. Aydin, I. Gokasar, and O. Kalan, "Matching algorithm for improving ride-sharing by incorporating route splits and social factors," *PLOS ONE*, vol. 15, no. 3, p. e0229674, 2020. https://doi.org/10.1371/journal.pone.0229674

[3] V. L. Zhao, M. Knoop, and M. Wang, "Two-dimensional vehicular movement modelling at intersections based on optimal control," *Transport. Res. Part B: Methodol.*, vol. 138, pp. 1–22, 2020. https://doi.org/10.1016/j.trb.2020.04.001

[4] C. Chai, Y. D. Wong, and X. Wang, "Safety evaluation of driver cognitive failures and driving errors on right-turn filtering movement at signalized road intersections based on fuzzy cellular automata (FCA) model," *Accid. Anal. Prev.*, vol. 104, pp. 156–164, 2017. https://doi.org/10.1016/j.aap.2017.04.026

[5] Z. Tao, X. Liu, H. Chen, and Z. Chen, "Group decision making with fuzzy linguistic preference relations via cooperative games method," *Comput. Ind. Eng.*, vol. 83, pp. 184–192, 2015. https://doi.org/10.1016/j.cie.2015.02.016

[6] B. Li, W. Xu, H. Xuan, and C. Xu, "Dynamic vehicle scheduling for working service network with dual demands," *J. Adv. Transp.*, p. 13, 2017. https://doi.org/10.1155/2017/7217309

[7] S. Lee, J. Turner, M. S. Daskin, T. Homem de Mello, and K. Smilowitz, "Improving fleet utilization for carriers by interval scheduling," *Eur. J. Oper. Res.*, vol. 218, no. 1, pp. 261–269, 2012. https://doi.org/10.1016/j.ejor.2011.10.019

[8] X. Liu, Y.-L. Chen, L. Y. Por, and C. S. Ku, "A systematic literature review of vehicle routing problems with time windows," *Sustainability*, vol. 15, no. 15, p. 12004, 2023. https://doi.org/10.3390/su151512004

[9] Y. Kergosien, C. Lenté, D. Piton, and J. C. Billaut, "A tabu search heuristic for the dynamic transportation of patients between care units," *Eur. J. Oper. Res.*, vol. 214, no. 2, pp. 442–452, 2011. https://doi.org/10.1016/j.ejor.2011.04.033

[10] S. Melo, R. Gomes, R. Abbasi, and A. Arantes, "Demand-responsive transport for urban mobility: Integrating mobile data analytics to enhance public transportation systems," *Sustainability*, vol. 16, no. 11, p. 4367, 2024. https://doi.org/10.3390/su16114367

[11] C. Park, J. Lee, and S. Y. Sohn, "Recommendation of feeder bus routes using neural network embedding-based optimization," *Transport. Res. Part A: Policy Pract.*, vol. 126, pp. 329–341, 2019. https://doi.org/10.1016/j.tra.2019.05.005

[12] B. Wang and I. Kim, "Short-term prediction for bike-sharing service using machine learning," *Transp. Res. Procedia*, vol. 34, pp. 171–178, 2018. https://doi.org/10.1016/j.trpro.2018.11.029

[13] N. Geržinič, N. van Oort, S. Hoogendoorn-Lanser, O. Cats, and S. Hoogendoorn, "Potential of on-demand services for urban travel," *Transp.*, vol. 50, no. 4, pp. 1289–1321, 2023. https://doi.org/10.1007/s11116-022-10278-9

[14] A. Corrêa, C. Silva, L. Xu, A. Brintrup, and S. Moniz, "Tunensearch: A hybrid transfer learning and local search approach for solving vehicle routing problems," *Comput. Oper. Res.*, vol. 190, p. 107433, 2026. https://doi.org/10.1016/j.cor.2026.107433

[15] M. Sami and K. Sara, "Intelligent transportation systems for sustainable urban environments," *Int. J. Adv. Nat. Sci. Eng. Res.*, vol. 7, no. 9, pp. 166–177, 2023. https://doi.org/10.59287/ijanser.1525

[16] M. Aamir, S. Masroor, Z. A. Ali, and B. T. Ting, "Sustainable framework for smart transportation system: A case study of Karachi," *Wirel. Pers. Commun.*, vol. 106, no. 2, pp. 27–40, 2019. https://doi.org/10.1007/s11277-019-06259-4

[17] P. Toth and D. Vigo, *Vehicle Routing: Problems, Methods, and Applications*. Society for Industrial and Applied Mathematics, 2014. https://doi.org/10.1137/1.9781611973594

[18] A. Ghiasi, O. Hussain, Z. S. Qian, and X. Li, "A mixed traffic capacity analysis and lane management model for connected automated vehicles: A Markov chain method," *Transp. Res. Part B: Methodol.*, vol. 106, pp. 266–292, 2017. https://doi.org/10.1016/j.trb.2017.09.022

[19] K. B. Spassov, "Optimization of on-demand public transportation," in *Proceedings of the 48th International Conference Applications of Mathematics in Engineering and Economics (AMEE 2022)*, 2022. https://doi.org/10.13140/RG.2.2.22483.25127

[20] Z. Cao, A. A. Ceder, and S. Zhang, "Real-time scheduling optimization for autonomous public transport vehicles to meet booking demands," *Transp. Res. Part E: Logist. Transp. Rev.*, vol. 200, p. 104202, 2025. https://doi.org/10.1016/j.tre.2025.104202

[21] J. Alonso-Mora, S. Samaranayake, A. Wallar, E. Frazzoli, and D. Rus, "On-demand high-capacity ride-sharing via dynamic trip-vehicle assignment," *Proc. Natl. Acad. Sci. USA*, vol. 114, no. 3, pp. 462–467, 2017. https://doi.org/10.1073/pnas.1611675114

[22] T. F. Golob, E. T. Canty, R. L. Gustafson, and J. E. Vitt, "An analysis of consumer preferences for a public transportation system," *Transp. Res.*, vol. 6, no. 1, pp. 81–102, 1972. https://doi.org/10.1016/0041-1647(72)90113-X

[23] L. Tang, "Artificial intelligence-based demand forecasting and route optimization modeling for public transportation in megacities," *Appl. Comput. Eng.*, vol. 169, pp. 159–167, 2025. https://doi.org/10.54254/2755-2721/2025.CH24538

[24] E. Azimirad and J. Haddadnia, "Design of an optimized fuzzy classifier system for urban traffic network," *J. Theor. Appl. Inform. Technol.*, vol. 41, no. 1, pp. 103–110, 2012. http://www.jatit.org/volumes/Vol41No1/14Vol41No1.pdf

[25] J. An, J. Zhao, Q. Liu, X. Qian, and J. Chen, "Self-constructed deep fuzzy neural network for traffic flow prediction," *Electronics*, vol. 12, no. 8, p. 1885, 2023. https://doi.org/10.3390/electronics12081885

[26] A. I. M. Almadi, R. E. Al Mamlook, Y. Almarhabi, I. Ullah, A. Jamal, and N. Bandara, "A fuzzy-logic approach based on driver decision making behavior modeling and simulation," *Sustainability*, vol. 14, no. 14, p. 8874, 2022. https://doi.org/10.3390/su14148874

[27] W. Pawlus, H. Karimi, and K. G. Robbersmyr, "A fuzzy logic approach to modeling a vehicle crash test," *Open Eng.*, vol. 3, no. 1, pp. 67–79, 2012. https://doi.org/10.2478/s13531-012-0032-2